symmetry

MDPI

Review

Lepton Asymmetries in Cosmology

Massimiliano Lattanzi [1,*] and Mauro Moretti [1,2]

[1] Istituto Nazionale di Fisica Nucleare, Sezione di Ferrara, Via Saragat 1, I-44122 Ferrara, Italy; mauro.moretti@unife.it
[2] Dipartimento di Fisica e Scienze della Terra, Università degli Studi di Ferrara, Via Saragat 1, I-44122 Ferrara, Italy
* Correspondence: lattanzi@fe.infn.it

Abstract: The cosmological lepton asymmetry, i.e., an excess of leptons over antileptons, is still only loosely constrained, and might be much larger than its tiny baryonic counterpart. If this is the case, charge neutrality requires the lepton asymmetries to be confined in the neutrino sector. We recall the observational effects of neutrino asymmetries on the abundance of light elements produced during Big Bang Nucleosynthesis and on the pattern of cosmic microwave background anisotropies. We point to the necessity of solving the neutrino transport equations, taking into account the effect of flavour oscillation, to derive general and robust constraints on lepton asymmetries. We review the current bounds and briefly discuss prospects for next-generation CMB experiments.

Keywords: lepton asymmetries; big bang nucleosynthesis; cosmic microwave background radiation

Citation: Lattanzi, M.; Moretti, M. Lepton Asymmetries in Cosmology. *Symmetry* **2024**, *16*, 1657. https://doi.org/10.3390/sym16121657

Academic Editors: Seokcheon Lee and Gansukh Tumurtushaa

Received: 25 November 2024
Revised: 11 December 2024
Accepted: 13 December 2024
Published: 15 December 2024

1. Introduction

One of the puzzling facts about our Universe is that it appears to be devoid of antimatter. This is traced back to a tiny (less than a part in a billion) baryon asymmetry that was generated in the primordial Universe in a process called baryogenesis. The conditions for baryogenesis to occur were elucidated by Sacharov in 1967, but the underlying mechanism is still unknown. Whatever the mechanism, sphaleron transitions in the early Universe are in general expected to produce a lepton asymmetry of the same order of the baryonic one [1–4]. In spite of this, several scenarios have been proposed where a small value of the baryon asymmetry can be generated together with large lepton asymmetries, see, e.g., [5–15]. Large lepton asymmetries can impact phase transitions in the early Universe [16], the generation of primordial magnetic fields [17], and the decoupling of WIMP dark matter [18]. They have also been proposed as a way to reconcile the sterile neutrino interpretation of anomalies observed at short baseline oscillation experiments with cosmological constraints on the radiation density in the early Universe [19,20]. Large lepton asymmetries can be in principle constrained by measurements of the abundances of light elements and by observations of anisotropies of the cosmic microwave background (CMB). Current constraints are, however, many order of magnitude weaker than the baryonic measurement. In the following, we will review present constraints and discuss prospects for future experiments.

2. Baryon and Lepton Asymmetries

The baryon asymmetry of the Universe can be quantified by the quantity $Y_B = (n_b - \overline{n}_b)/s$, where s is the entropy density, while n_b and $\overline{n}_b$ are the number densities of baryons and antibaryons, respectively. In the following, we will use a bar to denote the density of antiparticles. After baryogenesis, no net baryon number is generated, and the baryon excess per unit volume $n_b - \overline{n}_b$ scales with the cosmological scale factor a like a^3. Since entropy is conserved by the expansion, the entropy density also scales like a^3, and the baryon asymmetry Y_b is constant.

Well after the time of electron–positron annihilation, i.e., at temperatures $\ll$ MeV, the entropy density is related to the number density of photons n_γ by $s = 7.04 n_\gamma$. Today, evidence suggests that $\overline{n}_b \simeq 0$, and we can relate Y_b to the baryon-to-photon ratio $\eta_b \equiv n_b/n_\gamma$ through $Y_B = 0.14\eta_b$ for $T \ll$ MeV. The present CMB temperature $T_\gamma = T_{\rm CMB} = 2.73\,\mathrm{K}$, together with measurements of the baryon density from the observations of CMB anisotropies of the Planck satellite [21,22], implies $Y_b = (8.70 \pm 0.06) \times 10^{-11}$.

Given the charge neutrality of the Universe, the total asymmetry in the charged lepton sector should be compensated by the baryon asymmetry (we will not consider here the possibility that large and opposite asymmetries in the individual charged lepton families compensate to generate a tiny charge asymmetry). Thus, any large lepton asymmetry should be confined in the neutrino sector. Analogously to Y_B, we define the lepton asymmetry Y_L as

$$Y_L \equiv \sum_\alpha \left(\frac{n_{\ell_\alpha} - \overline{n}_{\ell_\alpha}}{s} + \frac{n_{\nu_\alpha} - \overline{n}_{\nu_\alpha}}{s} \right) \simeq \sum_\alpha \frac{n_{\nu_\alpha} - \overline{n}_{\nu_\alpha}}{s}\,, \tag{1}$$

where ℓ and ν denotes charged leptons and neutrinos, respectively, and $\alpha = e,\, \mu,\, \tau$. We further define Y_{ν_α} as the asymmetries in the individual neutrino flavours:

$$Y_{\nu_\alpha} \equiv \frac{n_{\nu_\alpha} - \overline{n}_{\nu_\alpha}}{s}\,. \tag{2}$$

As we shall discuss in more detail in the following sections, current observations are compatible with neutrino asymmetries much larger than the baryonic one.

3. Basic Concepts

In this section, we recall some concepts about cosmological evolution that will be useful in the following. The observable effects of lepton asymmetries crucially depend on the kinetics of the cosmological plasma when the temperature of the Universe is around 1 MeV (referred as the "MeV era"), corresponding to roughly 1 s after the end of inflation, thus we will mostly focus on that period. We will neglect for the moment the effect of neutrino flavour oscillations, that typically become active for $T < 10\,\mathrm{MeV}$, and will be discussed in Section 5.

At temperatures $T \gg 1\,\mathrm{MeV}$, but well below the muon mass $\sim 100\,\mathrm{MeV}$, the cosmological plasma is composed of protons, neutrons, photons, electrons/positrons and neutrinos/antineutrinos. At such times, the Universe was radiation-dominated, meaning that ultrarelativistic particles gave the dominant contribution to the total energy. In this case, the expansion follows the Friedmann equation for a radiation-dominated Universe [23]:

$$H(T) = \left(\frac{8\pi G}{3} \rho_{\rm rad} \right)^{1/2} = 1.66 \sqrt{g_*(T)}\, \frac{T^2}{m_{\rm pl}} \tag{3}$$

where $\rho_{\rm rad}$ is the energy density of ultrarelativistic particles ("radiation"), H is the Hubble parameter, i.e., the cosmic expansion rate, T is the temperature of the plasma, $m_{\rm pl}$ is the Planck mass, and the quantity $g_*(T)$ quantifies the contribution of particle species with $m \ll T$ to the total energy density (see Kolb and Turner [23] for the exact definition). For $1\,\mathrm{MeV} \lesssim T \lesssim 100\,\mathrm{MeV}$, $g_* = 43/4$.

The components of the plasma are kept in thermal equilibrium by standard model interactions. In particular, the weak interaction rate $\Gamma_w \sim G_F T^5$, where G_F is the Fermi constant. It is straightforward to see that the condition $\Gamma_w > H$ holds for $T \gg 1\,\mathrm{MeV}$, so that neutrinos are kept in flavour eigenstates and in equilibrium with the rest of the plasma, and their distribution functions are Fermi–Dirac with temperature T and chemical potentials μ_α:

$$f_{\nu_\alpha}(p) = \frac{1}{e^{\frac{p-\mu_\alpha}{T}} + 1} \quad \alpha = e,\, \mu,\, \tau\,. \tag{4}$$

Chemical equilibrium further implies that the chemical potential of antineutrinos is opposite to that of neutrinos, $\overline{\mu}_\alpha = -\mu_\alpha$. The dimensionless chemical potentials (degeneracy parameter) ξ_α are defined as $\xi_\alpha \equiv \mu_\alpha/T$. From the distribution functions, one can compute the number density n_ν and energy density ρ_ν of neutrinos as:

$$n_\nu = \frac{1}{(2\pi)^3}\int d^3p f_\nu(p)\,; \quad \rho_\nu = \frac{1}{(2\pi)^3}\int d^3p\, p f_\nu(p)\,. \tag{5}$$

and similarly for antineutrinos. Note that in the expression for the energy density we have approximated $E \simeq p$ for neutrinos at early times.

When the temperature drops below a few MeVs, the weak interaction rate becomes smaller than the expansion rate and neutrinos decouple from the cosmological plasma. Slightly after, at $T \sim m_e$, electrons and positrons annihilate away and transfer their entropy to the photons, increasing their temperature with respect to neutrinos. In the limit in which neutrino decoupling happens instantaneously, entropy conservation dictates that the neutrino temperature relative to the photons is $T_\nu/T_\gamma = (4/11)^{1/3}$ after decoupling. In reality, decoupling is not instantaneous, and neutrinos share some of the entropy transfer from the electrons/positrons. Moreover, more energetic neutrinos stay coupled for a longer time. The net result is that the process of decoupling imprints spectral distortions in the neutrino distribution functions, and that after decoupling neither their temperature or chemical potentials are strictly speaking well defined. However, the spectral distortions are very small, at least in the standard scenario; thus, for qualitative discussions, it can still be useful to think in term of thermal distribution functions. We will return in more detail on the topic of neutrino decoupling in the next section.

As we shall see below, cosmological observables are sensitive to the contribution of neutrinos to the total energy density. The energy density during the radiation dominated era and well after e^+e^- annihilation is usually parameterized in terms of the effective number of relativistic species $N_{\rm eff}$, which is the energy density of radiation other than photons, in units of the energy density of an instantaneously decoupled neutrino species (including antiparticles), with vanishing chemical potential. It is defined through [24]

$$\rho_{\rm rad} \equiv \rho_\gamma\left[1 + \frac{7}{8}\left(\frac{4}{11}\right)^{4/3} N_{\rm eff}\right]. \tag{6}$$

The definition is built in such a way that $N_{\rm eff} = 3$ if (i) there are no other light species other than photons and neutrinos, (ii) neutrinos have a thermal distribution with vanishing chemical potential, and (iii) decoupling is instantaneous. In the next sections we will discuss the impact of relaxing (ii) and (iii). We anticipate however that the standard theoretical prediction for $N_{\rm eff}$ for active neutrinos is $N_{\rm eff} = 3.044$.

For the moment, let us note that if the neutrino distribution is still thermal, but with nonzero chemical potential, then the sum of the neutrino and antineutrino energy densities for a single species is

$$\rho_{\nu+\overline{\nu}} = \left[1 + \frac{30}{7}\left(\frac{\xi}{\pi}\right)^2 + \frac{15}{7}\left(\frac{\xi}{\pi}\right)^4\right]\rho_{\nu+\overline{\nu}}|_{\xi=0}\,. \tag{7}$$

A chemical potential therefore produces an excess in $N_{\rm eff}$ given by:

$$\Delta N_{\rm eff}(\xi_\alpha) = \left[\frac{30}{7}\left(\frac{\xi_\alpha}{\pi}\right)^2 + \frac{15}{7}\left(\frac{\xi_\alpha}{\pi}\right)^4\right] \tag{8}$$

We conclude this section by noting that, in the case of a thermal spectrum, the neutrino asymmetry can be expressed in terms of the chemical potentials using $n_{\nu_\alpha} = (2\pi)^{-3} \int f_{\nu_\alpha} d^3p$:

$$Y_{\nu_\alpha} = \frac{T^3}{6\pi^2} \frac{\pi^2 \xi_\alpha + \xi_\alpha^3}{s} \simeq (3.5 \times 10^{-2}) \left(\xi_\alpha + \frac{\xi_\alpha^3}{\pi^2} \right), \tag{9}$$

where the last equality holds for temperatures $1\,\mathrm{MeV} \ll T \ll 100\,\mathrm{MeV}$. Then the primordial (i.e., at $T \gg 1\,\mathrm{MeV}$) lepton asymmetries can be parameterized through the primordial neutrino degeneracy parameters ξ_α.

Note that the relations in Equations (7)–(9) are exact. In fact, even if the number and energy densities of neutrino and antineutrino separately cannot be expressed in terms of elementary functions (they can however be expressed using polylogarithms), still the difference of the number densities (Equation (9)) and the sum of energy densities (Equations (7) and (8)) of neutrinos and antineutrinos take the simple forms reported above.

4. Cosmological Observables

Neutrino asymmetries could, in principle, leave an imprint in cosmological observables, in particular in the abundance of light elements and in the pattern of CMB anisotropies. We discuss these imprints here.

4.1. Light Element Abundances

Light elements—D, ^{3}He, ^{4}He, ^{7}Li—were produced in the early Universe, at temperatures $\sim 1\,\mathrm{MeV}$, in a process called Big Bang Nucleosynthesis (BBN). For what concerns cosmological parameters, the yield of light elements produced during BBN depends on the density of baryonic matter, that sets the total amount of baryons (protons and neutrons) available to build light nuclei, and on the thermal and expansion history during the MeV era, that sets the initial neutron-to-proton ratio (see below) and the time for which nuclear reactions are effective before the temperature of the Universe becomes too low. Public BBN codes like `PArthENoPE` [25–27] or `PRIMAT` [28] can be used to compute primordial abundances as a function of the relevant BBN parameters.

In the standard cosmological model, the thermal history—essentially the function $T(t)$—during the MeV era is fixed; the only free parameter would be an overall normalization of the temperature, that is set by the measurement of the present photon temperature, i.e., of the CMB temperature. The light elements abundances are thus determined only by the baryon density. This can be expressed in terms of the density parameter of baryons $\omega_b = \Omega_b h^2$, where $\Omega_b = \rho_b/\rho_c$ is the ratio of the baryon density to the critical density $\rho_c = 1.88 \times 10^{-29} h^2$ g cm^{-3}, and h is the Hubble constant in units of $100\,\mathrm{km s^{-1} Mpc^{-1}}$. The density parameter ω_b is constrained by measurements of the CMB anisotropies. The legacy data of the Planck satellite have allowed to determine ω_b at the subpercent level: $100\omega_b = 2.237 \pm 0.015$ at 68% CL. In extended models with a nonstandard value of N_{eff}, BBN is also affected by the expansion rate at a given time being modified due to the different amount of radiation at the right-hand side of Equation (3).

From the observational point of view, the primordial ^{4}He abundance can be be determined through recombination emission lines of helium and hydrogen in blue compact galaxies. Based on a compilation of recent results, the PDG reports [29], for the primordial mass fraction of ^{4}He, $Y_p \equiv \rho_{^4He}/\rho_b$:

$$Y_p = 0.245 \pm 0.003, \qquad (68\%\mathrm{CL}), \tag{10}$$

where the uncertainty includes both statistical and systematic errors, with the latter dominating. Deuterium is instead measured through high-resolution spectroscopy of high-

redshift, low-metallicity quasar absorption systems. The PDG recommended value for D/H, the D number abundance relative to H, is

$$\mathrm{D/H} = (2.547 \pm 0.029) \times 10^{-5}. \qquad (68\%\mathrm{CL})\,. \tag{11}$$

We now discuss the impact of neutrino asymmetries on light element abundances. As mentioned above, the outcome of BBN is sensitive to the relative abundance of neutrons and protons at the time when neutron-to-proton conversion processes freeze out ($T \simeq 0.8\,\mathrm{MeV}$), since this determines the "initial conditions" for the synthesis of light elements. In particular, the neutron-to-proton ratio n/p is set by the weak reactions

$$n + \nu_e \longleftrightarrow p + e^-\,, \tag{12}$$
$$n + e^+ \longleftrightarrow p + \overline{\nu}_e\,, \tag{13}$$
$$n \longleftrightarrow p + e^- + \overline{\nu}_e\,. \tag{14}$$

An asymmetry between electron neutrinos and antineutrinos will shift the equilibrium of these reactions and change the value of n/p at freeze-out. A positive chemical potential $\xi_{e,\mathrm{BBN}}$ for the electron neutrino at the time of BBN, i.e., a larger density of neutrinos, will shift the reactions towards the right and result in a smaller value for n/p. The opposite would happen for $\xi_{e,\mathrm{BBN}} < 0$. In fact, assuming thermal equilibrium, Pitrou et al. [28] find $n/p = (n/p)_{\xi_e=0} e^{-\xi_{e,\mathrm{BBN}}}$. Another effect comes from the increase in the total neutrino and antineutrino energy density associated to a chemical potential as in Equation (8). The extra energy density causes a faster expansion, i.e., a smaller age of the Universe at a given temperature. At the onset of BBN, corresponding to the time when deuterium synthesis starts ($T \simeq 0.07\,\mathrm{MeV}$), the neutron-to-proton ratio is smaller than its freeze-out value due to weak neutron decays. A faster expansion reduces the time elapsed between freeze-out and the onset of BBN, slightly increasing n/p. Note that this effect receives contributions from all neutrino flavours: a degeneracy in the μ or τ neutrinos does not alter beta reactions, but will still change the expansion rate. This increase is however quadratic in ξ, while the suppression in n/p at freeze out due to the altered chemical equilibrium of weak processes is exponential, so the latter dominates unless $\xi_e \ll \xi_{\mu,\tau}$.

The net effect of electron (anti)neutrino chemical potential on the abundances of light elements was estimated numerically in Pitrou et al. [28] using the PRIMAT code. For the helium-4 abundance Y_p they find:

$$Y_P(\xi_{\nu_e}) \simeq Y_P|_{\xi_e=0}\, e^{-0.96\xi_{\nu_e}}\,, \tag{15}$$

while for the deuterium abundance relative to hydrogen, D/H

$$D/H(\xi_{\nu_e}) \simeq D/H|_{\xi_e=0}\, e^{-0.53\xi_{\nu_e}}\,. \tag{16}$$

From these dependencies, it can be seen that percent measurements of Y_p and D/H as in Equations (10) and (11) would provide a similar sensitivity the the chemical potential of the electron neutrino.

4.2. CMB Anisotropies

The CMB photons have decoupled from baryons at early times ($T \sim 0.3\,\mathrm{eV}$, thus much after BBN), shortly after the time protons and electrons combined to form hydrogen atoms (a process oddly called hydrogen *re*combination), when the sudden drop in the density of free electrons made the Universe transparent to the propagation of light. The CMB displays small ($\sim 10^{-5}$) anisotropies, generated by acoustic oscillations of the photon-baryon fluid. The anisotropies trace correspondingly small fluctuations in the density and velocity of photons, and in the gravitational potentials, at the time of CMB decoupling, roughly 400,000 years after the end of inflation.

CMB anisotropies are also sensitive to neutrino chemical potentials. In fact, CMB observations allow to measure both $N_{\rm eff}$ and Y_p. Planck 2018 observations of the CMB anisotropies [22] (In this paragraph we quote numbers obtained using the information from both temperature and polarization anisotropies, and from reconstruction of the CMB lensing potential. This is the likelihood referred as *Planck* TT,TE,EE+lowE+lensing in the Planck papers.) constrain $N_{\rm eff} = 2.89 \pm 0.19$ (68% CL) when Y_p is computed consistently from $N_{\rm eff}$ and ω_b. If instead $N_{\rm eff}$ is fixed to the standard value 3.044, and Y_p is left free to vary, Planck data yield the constrain $Y_p = 0.239 \pm 0.013$ (68% CL). Note that this is a factor ~ 4 less constraining than the result from direct astrophysical measurements in Equation (10). Given that the sensitivity to both $N_{\rm eff}$ and Y_p stems from their effect on the damping tail (see below), it can be expected their estimates to be strongly correlated. Indeed, if both parameters are left free to vary, one obtains, at 68%CL, the looser constraints

$$N_{\rm eff} = 2.84^{+0.27}_{-0.32}\,, \tag{17}$$

$$Y_p = 0.247 \pm 0.018\,. \tag{18}$$

A graphical comparison of the constraints can be seen in Figure 1.

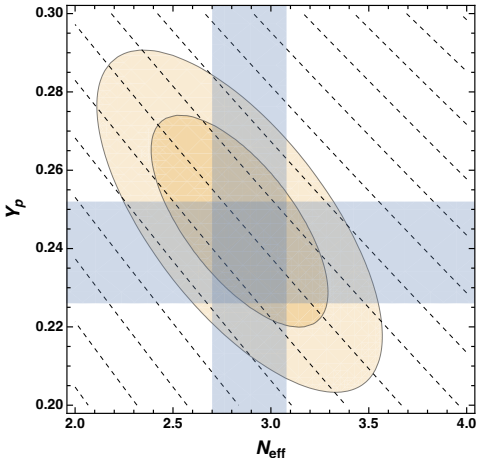

Figure 1. Constraints on $N_{\rm eff}$ and Y_p from Planck 2018 temperature, polarization and lensing data. The shaded yellow ellipses show the 68% and 95% regions when both $N_{\rm eff}$ and Y_p are left free to vary. The blue bands show constraints on each individual parameter when either $N_{\rm eff}$ is fixed to the standard value $N_{\rm eff}$ = 3.044 (for Y_p) or Y_p is computed according to the standard BBN picture (for $N_{\rm eff}$). The dashed lines are the curves of constant r_d/r_s, according to Equation (20).

We now discuss what makes CMB anistropies sensitive to $N_{\rm eff}$ and Y_p and then, in turn, to neutrino asymmetries. Small-scale fluctuations undergo diffusion damping (also known as Silk damping), resulting in an exponential suppression below the photon diffusion scale. The mean squared diffusion distance r_d^2 at recombination is

$$r_d^2 = \pi^2 \int_0^{a_*} \frac{da}{a^3 \sigma_T n_e H} F(\rho_b/\rho_\gamma)\,, \tag{19}$$

where a is the cosmological scale factor, a_* its value at CMB decoupling, σ_T is the Thomson cross-section, n_e is the density of free electrons, and the function F appears due to the directional and polarization dependence of Thomson scattering (see, e.g., [30] for the explicit expression). CMB observations show that the projected scale of the photon diffusion length is around 5 arcminutes.

The damping scale is sensitive to neutrino asymmetries in two ways. CMB decoupling happens after the end of the radiation-dominated era, but close enough that radiation still gives a nonnegligible contribution to the total density. The extra contribution to $N_{\rm eff}$ from Equation (8) will thus increase the expansion rate H and decrease the damping length as

$\sim 1/\sqrt{H}$. The density of free electrons n_e is instead sensitive to the helium abundance Y_p. In fact, since hydrogen and helium recombine at slightly different times, the evolution of free electron density depends on their relative abundance. Helium recombines earlier than hydrogen, due to its larger ionization energy, so that the density of free electrons decreases faster with larger helium fraction. This in turns increases the photon diffusion length. The recombination of helium happens so early that is a good approximation to consider it is completely finished when the CMB starts to decouple and diffusion damping is effective, so we can write $n_e \propto (1 - Y_p)$.

The Silk damping scale is projected to an angular scale that depends on the distance to CMB decoupling (and on the spatial curvature of the Universe if it is not assumed to be flat). This is only known with some uncertainty that would in principle prevent a precise determination of r_d from observations. However, as noted by Hou et al. [30], one can take the ratio of r_d with another characteristic length scale that is imprinted (after projection) in the CMB anisotropy pattern. Such a ratio would be independent of projection effects. The other length scale is the sound horizon at recombination r_s, i.e., the distance traveled by a sound wave until recombination. This distance sets the positions and the characteristic spacing of the peaks observed in the power spectrum of CMB anisotropies. The sound horizon $r_s \propto 1/H$, thus, the ratio $r_d/r_s \propto \sqrt{H} \propto (1 + cN_{\rm eff})^{1/4}$ where $c = (7/8)(4/11)^{4/3}$, and we have used Equations (3) and (6). Inserting also the dependence of n_e on Y_p, eventually one should expect $r_d/r_s \propto (1 + cN_{\rm eff})^{1/4}/\sqrt{1 - Y_p}$. This is basically confirmed by a more refined numerical analysis, with the only change that the exponent of the $1 + cN_{\rm eff}$ term is 0.28 rather than 0.25:

$$\frac{r_d}{r_s} \propto \frac{(1 + cN_{\rm eff})^{0.28}}{\sqrt{1 - Y_p}} \,. \tag{20}$$

Observations of the CMB small-scale anisotropies allow to pinpoint the ratio r_d/r_s quite precisely: the Planck 2018 results allow a determination at the few per mille level, as it can be inferred, e.g., from Table 2 of Aghanim et al. [22]. This is what allows to constrain $N_{\rm eff}$ and Y_p with their respective uncertainties. In order to obtain insight on how a determination of r_d/r_s implies for a neutrino chemical potential, we can Taylor expand Equation (20) around $\xi = 0$. Keeping terms up to order ξ^2, we obtain

$$\frac{r_d}{r_s}(\xi) = \left.\frac{r_d}{r_s}\right|_{\xi=0} \left(1 - 0.157\xi + 0.162\xi^2\right) . \tag{21}$$

where we have assumed that the chemical potentials of the three flavours are all equal. This implies, for the sensitivity $\Delta\xi$

$$\Delta\xi \simeq 6\frac{\Delta(r_d/r_s)}{r_d/r_s} \tag{22}$$

so that a few per mille determination of r_d/r_s corresponds to a sensitivity to values of $\xi \sim 10^{-2}$. Note that most of the sensitivity comes through Y_p: if we turn off the dependency on this parameter, the $r_d/r_s - \xi$ relation is quadratic in ξ at leading order, and the sensitivity to ξ is considerably degraded. Thus, although if we have assumed that the chemical potentials are the same, the relation in Equation (22) is still supposed to hold for the electron neutrino chemical potential even if this is not the case, as long as $|\xi_e| \gg |\xi_{\mu,\tau}|$. In fact, we have explicitly verified this in the case $\xi_\mu = \xi_\tau = 0$. In Figure 2, we plot the likelihood of ξ assuming a measurement of r_d/r_s with 10^{-3} accuracy, in the two cases $\xi_e \gtrsim \xi_{\mu,\tau}$ and $\xi_e = 0$. Specifically, considering an uncertainty $\sigma(r_d/r_s) = 10^{-3} - 3 \times 10^{-3}$, the 95% upper bound for $|\xi_e|$ (the likelihood does not depend on the sign of ξ at leading order, thus we quote sensitivity to $|\xi|$) falls in the range 0.012–0.04. If $\xi_e = 0$, the 95% upper bound for $|\xi_{\mu,\tau}|$ is instead in the range 0.20–0.35.

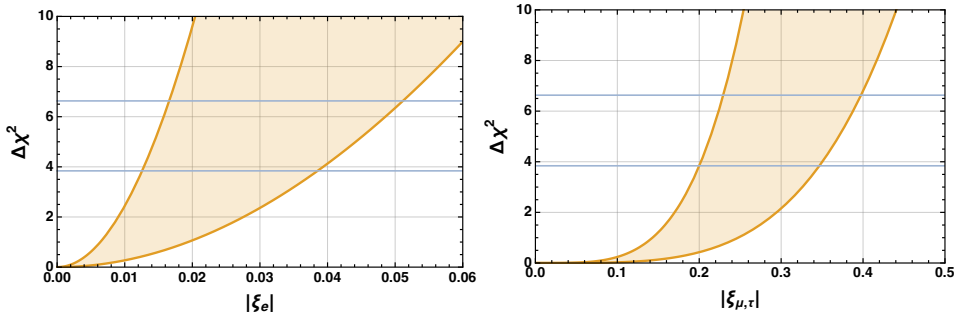

Figure 2. $\Delta\chi^2$ (relative to the case of vanishing chemical potentials), as a function of ξ. In both panels we assume a determination of the ratio r_d/r_s from CMB observations, with relative accuracy ranging from 10^{-3} (leftmost curve) to 3×10^{-3} (rightmost curve). The horizontal lines correspond to 95% and 99% frequentist CLs. (**Left**): case $\xi_e \gtrsim \xi_{\mu,\tau}$ (see text for details). (**Right**): case $\xi_e = 0$. Note the different scale in the horizontal axes of the two panels.

In this section, we have implicitly assumed that neutrino chemical potentials are still well-defined, or equivalently that neutrino distributions are still thermal, at the time of BBN and CMB. This is not however strictly the case since neutrino decoupling introduces spectral distortions. Moreover, even if the spectral distortions are small enough to make a description of the neutrino fluid in terms of (effective) temperature and chemical potentials, flavor oscillations allow to redistribute the asymmetries among the flavors. Thus, the chemical potentials discussed in this section are not necessarily equal to their primordial values. The relation between the primordial asymmetries and those at later times, relevant for BBN and CMB, is not trivial. This will be discussed in the next section.

5. Neutrino Transport

We have so far implicitly assumed that the effect of neutrino asymmetries is completely encoded in the neutrino chemical potentials. This is not however really the case, because chemical potential and temperature are well-defined only in thermal equilibrium, when the distribution functions have the form in Equation (4). While this is the case well before neutrino decoupling, i.e., for $T \gg 1\,\mathrm{MeV}$, it is not true at later times, neutrino decoupling being essentially a departure from equilibrium process. In order to obtain accurate predictions, one thus has to follow the evolution of the asymmetries themselves, Equation (2), which are always well defined. Note however that we are still allowed to refer to the degeneracy parameters at early times, when thermal equilibrium holds, as setting the initial conditions for the evolution of asymmetries.

Another complication comes from the fact that neutrinos undergo flavour oscillations. Even in the "standard" case of vanishing lepton asymmetries, a precision calculation of neutrino decoupling requires to account for the effect of neutrino oscillations. Such a calculation was first presented in Ref. [31], and other studies refined the analysis in the last decade [32–35]. The inclusion of neutrino flavour oscillations and QED finite temperature corrections to the plasma equation of state leads to the standard prediction $N_{\mathrm{eff}} = 3.044$.

Oscillations are typically active at $T \lesssim 10\,\mathrm{MeV}$. In fact, the oscillation length $L^{\mathrm{osc}} = 4\pi E/|\Delta m^2|$ for all pairs of mass eigenstates is larger than the Hubble length H^{-1} at temperatures above a few tens of MeVs. The intrinsically quantum nature of the process entails employing the density matrix formalism to describe the neutrino ensemble [36]. The diagonal elements of the density matrix in the flavour basis are the distribution functions, while the off-diagonal elements describe flavour coherence. The density matrices of neutrinos and antineutrinos ϱ and $\overline{\varrho}$ are evolved using the Quantum Kinetic Equations (QKEs).

Here, we give some details on the formalism of QKE for neutrino transport in the early Universe. See, e.g., Froustey et al. [33] for further details. The QKEs read:

$$\left(\frac{\partial}{\partial t} - Hp\frac{\partial}{\partial p}\right)\varrho = -i\left[\frac{\mathbb{M}_{\rm F}^2}{2p} - 2\sqrt{2}G_F p\left(\frac{\mathbb{E}_\ell + \mathbb{P}_\ell}{m_W^2} + \frac{4}{3}\frac{\mathbb{E}_\nu}{m_Z^2}\right) + \sqrt{2}G_F\mathcal{A},\, \varrho\right] + \mathcal{I} \quad (23a)$$

$$\left(\frac{\partial}{\partial t} - Hp\frac{\partial}{\partial p}\right)\overline{\varrho} = +i\left[\frac{\mathbb{M}_{\rm F}^2}{2p} - 2\sqrt{2}G_F p\left(\frac{\mathbb{E}_\ell + \mathbb{P}_\ell}{m_W^2} + \frac{4}{3}\frac{\mathbb{E}_\nu}{m_Z^2}\right) - \sqrt{2}G_F\mathcal{A},\, \varrho\right] + \overline{\mathcal{I}}\,. \quad (23b)$$

Here, H is the Hubble parameter, $\mathbb{M}_{\rm F}^2 = U\mathbb{M}^2U^\dagger$ with $\mathbb{M}$ the neutrino mass matrix in the mass basis and U the Pontecorvo–Maki–Nakagawa–Sakata (PMNS) matrix, $\mathbb{E}_\ell$ and $\mathbb{P}_\ell$ are the diagonal matrices of charged leptons+antileptons energy densities and pressures, $\mathbb{E}_\nu$ is similarly defined for neutrinos (note that $\mathbb{P}_\nu = \frac{1}{3}\mathbb{E}_\nu$ for relativistic neutrinos, hence the factor $4/3$ in front of the $\mathbb{E}_\nu$ term), $\mathcal{A}$ is the matrix of neutrino asymmetries:

$$\mathcal{A} = \mathbb{N}_\nu - \mathbb{N}_{\bar\nu} = \frac{1}{(2\pi)^3}\int(\varrho - \overline{\varrho})d^3p\,, \quad (24)$$

and $\mathcal{I}$ is the collision term, accounting for scattering with charged leptons, scatterings between neutrinos, neutrino pair production and annihilation.

We briefly comment on the physical meaning of each term appearing in the commutator at the right-hand side of the QKEs. The first term is the vacuum term, i.e., the neutrino kinetic term, that is diagonal in the mass basis. The remaining terms in the commutator, proportional to G_F, describe matter effects through the mean-field potential generated by interactions with the particles in the plasma. In particular, the term proportional to $\mathcal{A}$ is the neutrino/antineutrino asymmetric mean field potential arising from the $V-A$ Hamiltonian. Note that, in principle, a corresponding term for the charged leptons should appear in the QKEs, but it can be neglected given the expectation that charged lepton asymmetries should be small to ensure charge neutrality of the Universe.

Equation (23a,b) are supplemented by the continuity equation for the expanding Universe:

$$\rho + 3H(\rho + P) = 0\,, \quad (25)$$

where ρ and P are the total energy and pressure of the plasma.

The QKE are evolved numerically starting at high enough temperatures, $T \gg 1\,\mathrm{MeV}$, when weak processes keep neutrinos in thermal equilibrium and in flavor eigenstates. A suitable change of the time and momentum variables turns the QKE into ordinary differential equations. The diagonal elements of the density matrices at the initial time are therefore given by the Fermi–Dirac distributions (4) while the off-diagonal elements are zero.

In presence of lepton asymmetries, oscillations allow to transfer them between the different flavours. The impact of flavour mixing on the cosmological evolution of lepton asymmetries has been studied, at a varying level of detail, in several works in the last two decades. Here, we briefly summarize the current status, and refer the reader to Refs. [37–50] for further details. Flavour mixing tends to drive the asymmetries towards an equilibration, although this is not always reached in general. Dolgov et al. [40] were the first to note that oscillations often lead to equalization of the chemical potentials. In this case the constrain from ^{4}He abundance (see previous section) applies to all flavours. However, other analyses pointed out the equalization does not always happen, and that fine-tuned initial conditions can prevent it [38]. Also, the degree of equilibration depends on the value of the θ_{13} mixing angle [42,43]. Still, equalization of the μ and τ asymmetries has been for a long time thought to happen in general, given the early onset of fast $\mu-\tau$ oscillations. However, recent studies have argued that also $\mu-\tau$ equalization is not in general guaranteed [46,50]. Solving the QKEs for the neutrino transport is in any case

necessary to connect the primordial asymmetries, or equivalently the primordial chemical potentials, to the cosmological observables.

When oscillations are taken into account, initially large asymmetries do not necessarily lead to a large value of $N_{\rm eff}$ as it would be inferred by a naive application of Equation (8). The reason is an interplay between flavour mixing and collisions [41]. The approximate redistribution of the asymmetries caused by oscillations is associated to a reheating of the neutrinos. In other words, the extra entropy associated to the asymmetries is converted to a larger temperature. Then, if neutrinos are still thermally coupled to the plasma when oscillations are effective, collisions will further transfer this entropy, cooling the neutrinos and heating the plasma. In the limiting regime of perfect averaging of the chemical potentials (for the discussion in this paragraph we are neglecting neutrino spectral distortions generated during the evolution, thus assuming that chemical potentials are always well defined) occurring well before neutrino decoupling—which, we stress again, is not guaranteed to happen—neutrinos will end up sharing a common temperature with the plasma (before e^+e^- annihilation). Thus, the contribution of the asymmetries to $\Delta N_{\rm eff}$ is still given by Equation (8), just with all ξ_α equal to their common value. Given the functional dependence of $\Delta N_{\rm eff}$ on the ξ_α, the final value of $\Delta N_{\rm eff}$ will be smaller than its initial value (From the mathematical point of view, this is basically a consequence of $\Delta N_{\rm eff}$ being a convex function of the ξ_α's. Then the discrete version of Jensen's inequality implies that the $\Delta N_{\rm eff}$ computed with the average chemical potential is smaller that the average of $\Delta N_{\rm eff}$). If instead the entropy transfer from neutrinos to the plasma is not complete, one should take also into account the different temperatures; this is not captured by Equation (8) that assumes equal temperature between neutrinos and the plasma before e^+e^- annihilation. In any case, an accurate computation of the value of $N_{\rm eff}$ at the times of interest for BBN and CMB requires to solve the full neutrino transport equations. We illustrate these points in Figure 3.

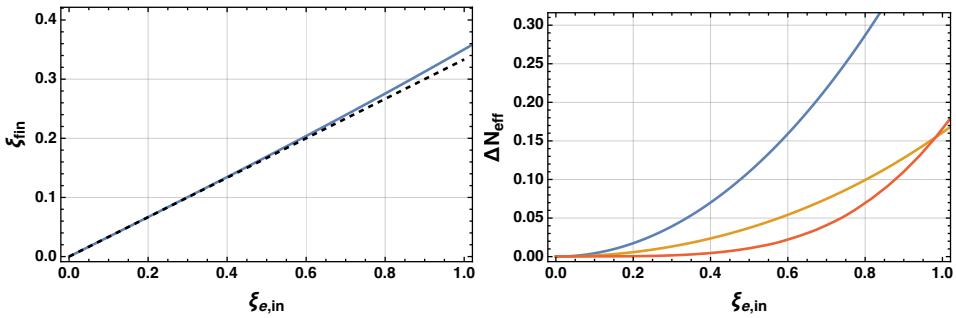

Figure 3. (**Left**): common value of the dimensionless chemical potential after equalization $\xi_{\rm fin}$ as a function of the electron neutrino chemical potential $\xi_{e,in}$ before equalization (solid blue line). We assume that perfect equalization occurs, i.e., $\xi_{e,fin} = \xi_{\mu,fin} = \xi_{\tau,fin} = \xi_{fin}$, and that it takes place well before neutrino decoupling. We use conservation of the total lepton asymmetry and of comoving energy to relate the initial temperature and chemical potentials to their final value, as in Section IIA of [50]. We further assume that $\xi_{\mu,in} = \xi_{\tau,in} = 0$. The dashed black line corresponds to $\xi_{\rm fin} = \xi_e/3$. The plot shows how the final chemical potential is very close to the average of the initial values. (**Right**): Initial (blue) and final (yellow) values of $\Delta N_{\rm eff}$ computed from Equation (8) with the corresponding chemical potentials. Comparison between the curves shows that the final $\Delta N_{\rm eff}$ can be sensibly smaller than its initial value. We also show, as the red curve, the value of $\Delta N_{\rm eff}$ derived from the full solution of the neutrino QKE with the same initial conditions [50] (the data used to reconstruct this curve are publicly available at https://doi.org/10.5281/zenodo.11123226 (accessed date: 15 November 2024)). This further shows that the assumptions of perfect equilibration of the asymmetries and thermalization with the plasma, used to derive the yellow curve, can still lead to a significant misestimation of $\Delta N_{\rm eff}$ as compared to the one obtained from the solution of the QKEs.

6. Current Constraints and Future Prospects

In this section, we review constraints on lepton asymmetries from current measurements of light element abundances and CMB anisotropies. We also discuss prospects for future experiments.

We will focus on results that have appeared in the last decade. See however Refs. [42–44,51–57] for previous analyses using various combinations of BBN, CMB and possibly other cosmological data. Most of these analyses assume flavour equilibration and a thermal neutrino spectrum, parametrising lepton asymmetries through a single chemical potential. The exception are Refs. [42–44] that follow the dynamics of the full neutrino distribution functions through the QKE formalism.

More recently, again under the assumption of perfect flavour equalization and negligible spectral distortions, Ref. [58] finds, analysing the Planck 2015 data [59], $\xi = -0.002^{+0.053}_{-0.060}$ at 68% CL (unless otherwise stated, all constraints in the following will be 68% CL). Note that this limit applies to the "late-time", i.e., after equalization, chemical potentials. Since however the total asymmetry is conserved, the above bound implies $Y_L < 2.1 \times 10^{-3}$. The constraint is mainly driven by the Planck sensitivity to the ^{4}He abundance. With the same assumptions, Ref. [28] finds, combining Planck 2015 with measurements of helium [60] and deuterium [61] abundances, $\xi = -0.001 \pm 0.016$ ($Y_L < 0.56 \times 10^{-3}$). Ref [62] derive instead joint constraints on a number of neutrino properties—mass, number of species, effective viscosity and speed of sound, chemical potential. In this extended model, they find $\xi < 0.05$ using Planck CMB data together with galaxy power spectrum measurements from BOSS and eBOSS.

Ref. [63] derives a constraint on primordial lepton asymmetries observing that these, if present at $T > 10^6$ GeV, would trigger a chiral plasma instability which sources helical hypermagnetic fields. This would in turn, after the electroweak phase transition, contribute to the baryon asymmetry of the Universe. In order to insure agreement with the observed baryon asymmetry, the individual chemical potentials should be $\xi < 9 \times 10^{-3}$. This bound naturally does not apply to asymmetries produced at $T < 10^6$ GeV.

Matsumoto et al. [64] have reported an anomalously low (3σ below the standard BBN prediction) measurement of the primordial Helium abundance from the EMPRESS survey, and noted how this determination, when combined with the deuterium measurement of Cooke et al. [61], implies a $\sim 2\sigma$ preference for a non-vanishing electron neutrino chemical potential: $\xi_e = 0.05^{+0.03}_{-0.02}$. Refs. [65,66] have further investigated the implications for lepton asymmetries of the EMPRESS result. Combining this with CMB data from Planck, Ref. [66] finds $\xi = 0.043 \pm 0.015$ [$Y_L = (1.5 \pm 0.5) \times 10^{-3}$], i.e., the evidence for a nonzero lepton asymmetry strenghtens to 3σ. Using instead the PDG recommended value for the helium abundance [67] they find a value consistent with zero, $\xi = 0.008 \pm 0.013$ [$Y_L = (0.28 \pm 0.46) \times 10^{-3}$]. Ref. [65] similarly reaches the conclusion that, taken at face value, the EMPRESS results suggest that today's lepton asymmetry is large.

Recently, the authors of Ref. [50] have argued that a detailed treatment of the evolution of neutrino asymmetries in the MeV era is necessary to derive meaningful constraints from primordial abundances and CMB measurements. Their analysis indeed shows that present data still allow lepton asymmetries to be very large, even in the electron neutrino sector.

Next-generation CMB experiments targeting anisotropies at small scales, like Simons Observatory [68] or CMB-S4 [69] will bring additional information to constrain neutrino asymmetries. They are expected to provide precise measurements of the damping tail of the CMB power spectrum, thus yielding strong constraints on $N_{\rm eff}$ and Y_p. For example, treating the two parameters as independent, CMB-S4 might measure $N_{\rm eff}$ and Y_p with an uncertainty of 0.08 and 0.005, respectively, corresponding to $\sim$ 3% and 2% accuracy (see Table 4-2 in Ref [70]). In particular, the sensitivity to Y_p will improve by a factor 5 over current CMB measurements (for comparison, Planck 2018 yields $Y_p = 0.241 \pm 0.025$), becoming competitive with astrophysical measurements (again, compare with the PDG-21 value $Y_p = 0.245 \pm 0.003$). Ref. [66] finds that CMB-S4 might be able to put constraints on ξ below the 10^{-2} level, assuming equalization of the asymmetries. Ref. [50] has further

shown that future CMB experiments will provide significant constraints even in the most general case when equalization is not assumed to occur.

Given the aforementioned EMPRESS hint for a lepton asymmetry 7 orders of magnitude larger than the baryon asymmetry, one might wonder how such a large difference might be produced in the context of baryogenesis scenarios. Even disregarding the EMPRESS result, the enhanced sensitivity of future CMB experiments still "only" allows to probe values of lepton asymmetries many orders of magnitude larger than the baryonic one, making natural to ask the same question. As briefly mentioned in the introduction, in standard baryogenesis, electroweak sphalerons are expected to roughly equilibrate Y_B and Y_L. This can be avoided if the lepton asymmetries are generated below the electroweak phase transition, when sphalerons are inactive. This is however unlikely in the standard model, where $T_{\rm EW}\sim$100 GeV. In Ref. [6], such a situation is instead realized in a supersymmetric implementation of the Affleck–Dine mechanism [71], where the large lepton asymmetries prevent the restoration of the electroweak symmetry at all times after inflation, suppressing sphaleron transitions. Ref. [9] has shown that a large Y_B/Y_L ratio can arise in the minimal supersymmetric model (MSSM) if the two asymmetries are both generated through the Affleck–Dine mechanism, but along different directions of the MSSM scalar potential. Other possibilities to generate a lepton asymmetry below the freeze-out of sphaleron conversion are the decay of topological defects [7], freeze-in leptogenesis [12,13], resonant leptogenesis [11,14], and Q-ball decays [10,15]. In Ref. [8] it was instead pointed out that, within the standard model, a large electron neutrino asymmetry is consistent with a small baryon asymmetry if the total lepton asymmetry is zero (see also [72] for a realization of this scenario in the framework of leptogenesis). This scenario would hint to the existence of new flavour physics in the lepton sector.

We conclude by raising two issues that, in our opinion, should be addressed by future studies. Most of the analyses discussed here model the effect of neutrino asymmetries on cosmological observables in terms of chemical potentials. As mentioned above, a neutrino chemical potential is not well-defined after neutrino decoupling. It might however be the case that, given the sensitivity of current and future experiments, the effect of spectral distortions might be captured with sufficient accuracy by a description in terms of an effective temperature and chemical potentials. Most of the analyses, with some notable exceptions, also assume that flavor oscillations equalize the asymmetries before BBN. This is, in our opinion, a delicate point since this equalization is not guaranteed to occur, and the relation between the late-time asymmetries (even if these can be effectively summarized by effective chemical potentials) and their primordial values is in general non-trivial. Both these points warrant further investigations.

Author Contributions: Conceptualization, M.L.; investigation, M.L.; writing—original draft preparation, M.L.; writing—review and editing, M.L. and M.M. All authors have read and agreed to the published version of the manuscript.

Funding: M.L. acknowledges the financial support from the INFN InDark initiative and from the COSMOS network through the ASI (Italian Space Agency) Grants 2016-24-H.0 and 2016-24-H.1-2018, as well as 2020-9-HH.0 (participation in LiteBIRD, phase A). M.L. is partially funded by the European Union (ERC, RELiCS, project number 101116027).

Data Availability Statement: No new data were created in this study. The data analyzed in Figure 1 have been obtained from the following resources available in the public domain: Zenodo repository at https://doi.org/10.5281/zenodo.11123226 (accessed date: 15 November 2024), reference number DOI: 10.5281/zenodo.11123226.

Conflicts of Interest: The authors declare no conflicts of interest.

Abbreviations

The following abbreviations are used in this manuscript:

CMB	Cosmic Microwave Background
BBN	Big Bang Nucleosynthesis
QKE	Quantum Kinetic Equations

References

1. Kuzmin, V.A.; Rubakov, V.A.; Shaposhnikov, M.E. On the Anomalous Electroweak Baryon Number Nonconservation in the Early Universe. *Phys. Lett. B* **1985**, *155*, 36. [CrossRef]
2. Khlebnikov, S.Y.; Shaposhnikov, M.E. The Statistical Theory of Anomalous Fermion Number Nonconservation. *Nucl. Phys. B* **1988**, *308*, 885–912. [CrossRef]
3. Harvey, J.A.; Turner, M.S. Cosmological baryon and lepton number in the presence of electroweak fermion number violation. *Phys. Rev. D* **1990**, *42*, 3344–3349. [CrossRef] [PubMed]
4. Dreiner, H.K.; Ross, G.G. Sphaleron erasure of primordial baryogenesis. *Nucl. Phys. B* **1993**, *410*, 188–216. [CrossRef]
5. Dolgov, A.D.; Kirilova, D.P. On particle creation by a time dependent scalar field. *Sov. J. Nucl. Phys.* **1990**, *51*, 172–177.
6. Casas, A.; Cheng, W.Y.; Gelmini, G. Generation of large lepton asymmetries. *Nucl. Phys. B* **1999**, *538*, 297–308. [CrossRef]
7. Bajc, B.; Riotto, A.; Senjanovic, G. Large lepton number of the universe and the fate of topological defects. *Phys. Rev. Lett.* **1998**, *81*, 1355–1358. [CrossRef]
8. March-Russell, J.; Murayama, H.; Riotto, A. The Small observed baryon asymmetry from a large lepton asymmetry. *J. High Energy Phys. JHEP* **1999**, *11*, 015. [CrossRef]
9. McDonald, J. Naturally large cosmological neutrino asymmetries in the MSSM. *Phys. Rev. Lett.* **2000**, *84*, 4798–4801. [CrossRef]
10. Kawasaki, M.; Takahashi, F.; Yamaguchi, M. Large lepton asymmetry from Q balls. *Phys. Rev. D* **2002**, *66*, 043516. [CrossRef]
11. Pilaftsis, A.; Underwood, T.E.J. Resonant leptogenesis. *Nucl. Phys. B* **2004**, *692*, 303–345. [CrossRef]
12. Asaka, T.; Shaposhnikov, M. The νMSM, dark matter and baryon asymmetry of the universe. *Phys. Lett. B* **2005**, *620*, 17–26. [CrossRef]
13. Asaka, T.; Blanchet, S.; Shaposhnikov, M. The nuMSM, dark matter and neutrino masses. *Phys. Lett. B* **2005**, *631*, 151–156. [CrossRef]
14. Borah, D.; Dasgupta, A. Large neutrino asymmetry from TeV scale leptogenesis. *Phys. Rev. D* **2023**, *108*, 035015. [CrossRef]
15. Kawasaki, M.; Murai, K. Lepton asymmetric universe. *J. Cosmol. Astropart. Phys. JCAP* **2022**, *08*, 041. [CrossRef]
16. Schwarz, D.J.; Stuke, M. Lepton asymmetry and the cosmic QCD transition. *J. Cosmol. Astropart. Phys. JCAP* **2009**, *11*, 025. [CrossRef]
17. Semikoz, V.B.; Sokoloff, D.D.; Valle, J.W.F. Is the baryon asymmetry of the Universe related to galactic magnetic fields? *Phys. Rev. D* **2009**, *80*, 083510. [CrossRef]
18. Stuke, M.; Schwarz, D.J.; Starkman, G. WIMP abundance and lepton (flavour) asymmetry. *J. Cosmol. Astropart. Phys. JCAP* **2012**, *03*, 040. [CrossRef]
19. Mirizzi, A.; Saviano, N.; Miele, G.; Serpico, P.D. Light sterile neutrino production in the early universe with dynamical neutrino asymmetries. *Phys. Rev. D* **2012**, *86*, 053009. [CrossRef]
20. Saviano, N.; Mirizzi, A.; Pisanti, O.; Serpico, P.D.; Mangano, G.; Miele, G. Multi-momentum and multi-flavour active-sterile neutrino oscillations in the early universe: Role of neutrino asymmetries and effects on nucleosynthesis. *Phys. Rev. D* **2013**, *87*, 073006. [CrossRef]
21. Aghanim, N.; Akrami, Y.; Arroja, F.; Ashdown, M.; Aumont, J.; Baccigalupi, C.; Ballardini, M.; Banday, A.J.; Barreiro, R.B.; Bartolo, N.; et al. Planck 2018 results. I. Overview and the cosmological legacy of Planck. *Astron. Astrophys.* **2020**, *641*, A1. [CrossRef]
22. Planck Collaboration; Aghanim, N.; Akrami, Y.; Ashdown, M.; Aumont, J.; Baccigalupi, C.; Ballardini, M.; Banday, A.J.; Barreiro, R.B.; Bartolo, N.; et al. Planck 2018 results. VI. Cosmological parameters. *Astron. Astrophys.* **2020**, *641*, A6; Erratum in *Astron. Astrophys.* **2021**, *652*, C4. [CrossRef]
23. Kolb, E.W.; Turner, M.S. *The Early Universe*; Taylor & Francis: London, UK, 1990.
24. Lesgourgues, J.; Mangano, G.; Miele, G.; Pastor, S. *Neutrino Cosmology*; Cambridge University Press: Cambridge, UK, 2013.
25. Pisanti, O.; Cirillo, A.; Esposito, S.; Iocco, F.; Mangano, G.; Miele, G.; Serpico, P.D. PArthENoPE: Public Algorithm Evaluating the Nucleosynthesis of Primordial Elements. *Comput. Phys. Commun.* **2008**, *178*, 956–971. [CrossRef]
26. Consiglio, R.; de Salas, P.F.; Mangano, G.; Miele, G.; Pastor, S.; Pisanti, O. PArthENoPE reloaded. *Comput. Phys. Commun.* **2018**, *233*, 237–242. [CrossRef]
27. Gariazzo, S.F.; de Salas, P.; Pisanti, O.; Consiglio, R. PArthENoPE revolutions. *Comput. Phys. Commun.* **2022**, *271*, 108205. [CrossRef]
28. Pitrou, C.; Coc, A.; Uzan, J.P.; Vangioni, E. Precision big bang nucleosynthesis with improved Helium-4 predictions. *Phys. Rept.* **2018**, *754*, 1–66. [CrossRef]
29. Navas, S.; Amsler, C.; Gutsche, T.; Hanhart, C.; Hernández-Rey, J.J.; Lourenço, C.; Masoni, A.; Mikhasenko, M.; Mitchell, R.E.; Patrignani, C.; et al. Review of particle physics. *Phys. Rev. D* **2024**, *110*, 030001. [CrossRef]

30. Hou, Z.; Keisler, R.; Knox, L.; Millea, M.; Reichardt, C. How Massless Neutrinos Affect the Cosmic Microwave Background Damping Tail. *Phys. Rev. D* **2013**, *87*, 083008. [CrossRef]
31. Mangano, G.; Miele, G.; Pastor, S.; Pinto, T.; Pisanti, O.; Serpico, P.D. Relic neutrino decoupling including flavor oscillations. *Nucl. Phys. B* **2005**, *729*, 221–234. [CrossRef]
32. de Salas, P.F.; Pastor, S. Relic neutrino decoupling with flavour oscillations revisited. *J. Cosmol. Astropart. Phys. JCAP* **2016**, *07*, 051. [CrossRef]
33. Froustey, J.; Pitrou, C.; Volpe, M.C. Neutrino decoupling including flavour oscillations and primordial nucleosynthesis. *J. Cosmol. Astropart. Phys. JCAP* **2020**, *12*, 015. [CrossRef]
34. Akita, K.; Yamaguchi, M. A precision calculation of relic neutrino decoupling. *J. Cosmol. Astropart. Phys. JCAP* **2020**, *08*, 012. [CrossRef]
35. Bennett, J.J.; Buldgen, G.; De Salas, P.F.; Drewes, M.; Gariazzo, S.; Pastor, S.; Wong, Y.Y.Y. Towards a precision calculation of $N_{\rm eff}$ in the Standard Model II: Neutrino decoupling in the presence of flavour oscillations and finite-temperature QED. *J. Cosmol. Astropart. Phys. JCAP* **2021**, *04*, 073. [CrossRef]
36. Sigl, G.; Raffelt, G. General kinetic description of relativistic mixed neutrinos. *Nucl. Phys. B* **1993**, *406*, 423–451. [CrossRef]
37. Bell, N.F.; Volkas, R.R.; Wong, Y.Y.Y. Relic neutrino asymmetry evolution from first principles. *Phys. Rev. D* **1999**, *59*, 113001. [CrossRef]
38. Pastor, S.; Raffelt, G.G.; Semikoz, D.V. Physics of synchronized neutrino oscillations caused by selfinteractions. *Phys. Rev. D* **2002**, *65*, 053011. [CrossRef]
39. Wong, Y.Y.Y. Analytical treatment of neutrino asymmetry equilibration from flavor oscillations in the early universe. *Phys. Rev. D* **2002**, *66*, 025015. [CrossRef]
40. Dolgov, A.D.; Hansen, S.H.; Pastor, S.; Petcov, S.T.; Raffelt, G.G.; Semikoz, D.V. Cosmological bounds on neutrino degeneracy improved by flavor oscillations. *Nucl. Phys. B* **2002**, *632*, 363–382. [CrossRef]
41. Pastor, S.; Pinto, T.; Raffelt, G.G. Relic density of neutrinos with primordial asymmetries. *Phys. Rev. Lett.* **2009**, *102*, 241302. [CrossRef]
42. Mangano, G.; Miele, G.; Pastor, S.; Pisanti, O.; Sarikas, S. Updated BBN bounds on the cosmological lepton asymmetry for non-zero θ_{13}. *Phys. Lett. B* **2012**, *708*, 1–5. [CrossRef]
43. Mangano, G.; Miele, G.; Pastor, S.; Pisanti, O.; Sarikas, S. Constraining the cosmic radiation density due to lepton number with Big Bang Nucleosynthesis. *JCAP* **2011**, *03*, 035. [CrossRef]
44. Castorina, E.; Franca, U.; Lattanzi, M.; Lesgourgues, J.; Mangano, G.; Melchiorri, A.; Pastor, S. Cosmological lepton asymmetry with a nonzero mixing angle θ_{13}. *Phys. Rev. D* **2012**, *86*, 023517. [CrossRef]
45. Barenboim, G.; Park, W.I. Impact of CP-violation on neutrino lepton number asymmetries revisited. *Phys. Lett. B* **2017**, *765*, 371–376. [CrossRef]
46. Barenboim, G.; Kinney, W.H.; Park, W.I. Resurrection of large lepton number asymmetries from neutrino flavor oscillations. *Phys. Rev. D* **2017**, *95*, 043506. [CrossRef]
47. Barenboim, G.; Kinney, W.H.; Park, W.I. Flavor versus mass eigenstates in neutrino asymmetries: Implications for cosmology. *Eur. Phys. J. C* **2017**, *77*, 590. [CrossRef]
48. Gava, J.; Volpe, C. CP violation effects on the neutrino degeneracy parameters in the Early Universe. *Nucl. Phys. B* **2010**, *837*, 50–60; Erratum in *Nucl. Phys. B* **2020**, *957*, 115035. [CrossRef]
49. Johns, L.; Mina, M.; Cirigliano, V.; Paris, M.W.; Fuller, G.M. Neutrino flavor transformation in the lepton-asymmetric universe. *Phys. Rev. D* **2016**, *94*, 083505. [CrossRef]
50. Froustey, J.; Pitrou, C. Constraints on primordial lepton asymmetries with full neutrino transport. *Phys. Rev. D* **2024**, *110*, 103551. [CrossRef]
51. Lesgourgues, J.; Pastor, S. Cosmological implications of a relic neutrino asymmetry. *Phys. Rev. D* **1999**, *60*, 103521. [CrossRef]
52. Lattanzi, M.; Ruffini, R.; Vereshchagin, G.V. Joint constraints on the lepton asymmetry of the universe and neutrino mass from the wilkinson microwave anisotropy probe. *Phys. Rev. D* **2005**, *72*, 063003. [CrossRef]
53. Simha, V.; Steigman, G. Constraining The Universal Lepton Asymmetry. *J. Cosmol. Astropart. Phys. JCAP* **2008**, *08*, 011. [CrossRef]
54. Popa, L.A.; Vasile, A. WMAP 5-year constraints on lepton asymmetry and radiation energy density: Implications for Planck. *J. Cosmol. Astropart. Phys. JCAP* **2008**, *06*, 028. [CrossRef]
55. Shiraishi, M.; Ichikawa, K.; Ichiki, K.; Sugiyama, N.; Yamaguchi, M. Constraints on neutrino masses from WMAP5 and BBN in the lepton asymmetric universe. *J. Cosmol. Astropart. Phys. JCAP* **2009**, *07*, 005. [CrossRef]
56. Schwarz, D.J.; Stuke, M. Does the CMB prefer a leptonic Universe? *New J. Phys.* **2013**, *15*, 033021. [CrossRef]
57. Caramete, A.; Popa, L.A. Cosmological evidence for leptonic asymmetry after Planck. *J. Cosmol. Astropart. Phys. JCAP* **2014**, *02*, 012. [CrossRef]
58. Oldengott, I.M.; Schwarz, D.J. Improved constraints on lepton asymmetry from the cosmic microwave background. *EPL* **2017**, *119*, 29001. [CrossRef]
59. Planck Collaboration; Aghanim, N.; Arnaud, M.; Ashdown, M.; Aumont, J.; Baccigalupi, C.; Banday, A.J.; Barreiro, R.B.; Bartlett, J.G.; Bartolo, N.; et al. Planck 2015 results. XI. CMB power spectra, likelihoods, and robustness of parameters. *Astron. Astrophys.* **2016**, *594*, A11. [CrossRef]

60. Aver, E.; Olive, K.A.; Skillman, E.D. The effects of He I λ10830 on helium abundance determinations. *J. Cosmol. Astropart. Phys. JCAP* **2015**, *07*, 011. [CrossRef]
61. Cooke, R.J.; Pettini, M.; Steidel, C.C. One Percent Determination of the Primordial Deuterium Abundance. *Astrophys. J.* **2018**, *855*, 102. [CrossRef]
62. Kumar, S.; Nunes, R.C.; Yadav, P. Updating non-standard neutrinos properties with Planck-CMB data and full-shape analysis of BOSS and eBOSS galaxies. *J. Cosmol. Astropart. Phys. JCAP* **2022**, *09*, 060. [CrossRef]
63. Domcke, V.; Kamada, K.; Mukaida, K.; Schmitz, K.; Yamada, M. New Constraint on Primordial Lepton Flavor Asymmetries. *Phys. Rev. Lett.* **2023**, *130*, 261803. [CrossRef] [PubMed]
64. Matsumoto, A.; Ouchi, M.; Nakajima, K.; Kawasaki, M.; Murai, K.; Motohara, K.; Harikane, Y.; Ono, Y.; Kushibiki, K.; Koyama, S.; et al. EMPRESS. VIII. A New Determination of Primordial He Abundance with Extremely Metal-poor Galaxies: A Suggestion of the Lepton Asymmetry and Implications for the Hubble Tension. *Astrophys. J.* **2022**, *941*, 167. [CrossRef]
65. Burns, A.K.; Tait, T.M.P.; Valli, M. Indications for a Nonzero Lepton Asymmetry from Extremely Metal-Poor Galaxies. *Phys. Rev. Lett.* **2023**, *130*, 131001. [CrossRef]
66. Escudero, M.; Ibarra, A.; Maura, V. Primordial lepton asymmetries in the precision cosmology era: Current status and future sensitivities from BBN and the CMB. *Phys. Rev. D* **2023**, *107*, 035024. [CrossRef]
67. Particle Data Group; Zyla, P.; Barnett, R.M.; Beringer, J.; Dahl, O.; Dwyer, D.A.; Groom, D.E.; Lin, C.J.; Lugovsky, K.S.; Pianori, E.; et al. Review of Particle Physics. *Prog. Theor. Exp. Phys. PTEP* **2022**, *2022*, 083C01. [CrossRef]
68. Ade, P.; Aguirre, J.; Ahmed, Z.; Aiola, S.; Ali, A.; Alonso, D.; Alvarez, M.A.; Arnold, K.; Ashton, P.; Austermann, J.; et al. The Simons Observatory: Science goals and forecasts. *J. Cosmol. Astropart. Phys. JCAP* **2019**, *02*, 056. [CrossRef]
69. Abazajian, K.; Addison, G.E.; Adshead, P.; Ahmed, Z.; Akerib, D.; Ali, A.; Allen, S.W.; Alonso, D.; Alvarez, M.; Amin, M.A.; et al. CMB-S4: Forecasting Constraints on Primordial Gravitational Waves. *Astrophys. J.* **2022**, *926*, 54. [CrossRef]
70. Abazajian, K.N.; Adshead, P.; Ahmed, Z.; Allen, S.W.; Alonso, D.; Arnold, K.S.; Baccigalupi, C.; Bartlett, J.G.; Battaglia, N.; Benson, B.A.; et al. *CMB-S4 Science Book*, 1st ed.; 2016. http://arxiv.org/abs/1610.02743
71. Affleck, I.; Dine, M. A New Mechanism for Baryogenesis. *Nucl. Phys. B* **1985**, *249*, 361–380. [CrossRef]
72. Gu, P.H. Large Lepton Asymmetry for Small Baryon Asymmetry and Warm Dark Matter. *Phys. Rev. D* **2010**, *82*, 093009. [CrossRef]